Overbounding GNSS/INS Integration with Uncertain GNSS Gauss-Markov Error Parameters

Omar García Crespillo[1], Mathieu Joerger[2], Steve Langel[3]
[1]Institute of Communications and Navigation, German Aerospace Center (DLR)
[2]Department of Aerospace and Ocean Engineering, Virginia Tech
[3]Department of Communications, SIGINT and PNT, The MITRE Corporation

***Abstract*—The integration of GNSS with Inertial Navigation Systems (INS) has the potential to achieve high levels of continuity and availability as compared to standalone GNSS and therefore to satisfy stringent navigation requirements. However, robustly accounting for time-correlated measurement errors is a challenge when designing the Kalman filter (KF) used for GNSS/INS coupling. In particular, if the error processes are not fully known, the KF estimation error covariance can be misleading, which is problematic in safety-critical applications. In this paper, we design a GNSS/INS integration scheme that guarantees upper bounds on the estimation error variance assuming that measurement errors are first-order Gauss-Markov processes with parameters only known to reside within pre-established bounds. We evaluate the filter performance and guaranteed estimation by covariance analysis for a simulated precision approach procedure.**

***Index Terms*—Overbounding, Kalman filtering, GNSS, Inertial Systems, Guaranteed estimation, Precision Approach, Gauss Markov Process, Colored Noise, ARAIM**

I. Introduction

The demand for increased levels of autonomy in safety- and liability-critical transportation applications motivates the need for high-integrity navigation solutions. The combination of GNSS and Inertial Navigation Systems (INS) has been used since the 1990s in avionic systems as part of the Aircraft-Based Augmentation Systems (ABAS). It has also become a baseline approach for applications in challenging land, air, and sea environments, for example in autonomous ground vehicles and commercial quadcopters. GNSS/INS can potentially achieve high levels of continuity and availability as compared to standalone GNSS. However, providing a rigorous assessment of GNSS/INS integrity still poses unanswered challenges.

Fault detection algorithms have been developed to address sensor faults in integrated GNSS/INS schemes using a Kalman filter (KF) [1, 2, 3, 4]. However, there is no widely adopted approach to account for time-varying sensor errors when the structure of the error time correlation is uncertain. For example, assuming that sensor errors follow a Gauss-Markov Process (GMP), how should one account for an unknown GMP time constant? Robust estimators are a promising solution when dealing with mis-modeled errors in GNSS [5] and GNSS/INS positioning [6, 7], but no rigorous quantification of their estimation error is currently available and therefore they cannot readily be implemented in safety critical applications. Existing error overbounding techniques used for snapshot GNSS positioning [8] do not account for measurement error correlation and therefore are not guaranteed to overbound the positioning error distribution when used in a sequential estimation context.

Correlated error processes affect GNSS pseudoranges, IMU specific force, and IMU angular rate measurements. These errors have a substantial impact on the performance of the KF, and state estimate variance can be misleading if these errors are not properly modelled. Proper characterization of correlated errors can be a difficult task. For instance, in GNSS, the pseudorange error is an accumulation of multiple error sources including orbit, clock, atmospheric (ionospheric and tropospheric) and multipath, whose stochastic behavior depends upon complex system processes and a changing environment.

In [9, 10], we provided a solution for overbounding sequential estimation errors in the presence of Gauss-Markov (GM) error processes with unknown but bounded time constants and driving noises. In this paper, we apply the methodology in [9] to design a GNSS/INS Kalman filter so that the navigation estimation error is properly overbounded by the KF covariance for the states of interest when the error model parameters are not fully known. First, we revisit the overbounding process in [9]. The different GNSS error sources are then modeled using different ranges of correlation time constants. We describe the error models provided in aviation standards, in the ARAIM Working Group C, and in recent publications that address sequential estimation for high-integrity navigation. We then design a KF that includes augmented states for each of the time-correlated GNSS and IMU measurements. This GNSS/INS Kalman filter is implemented in a realistic simulated aircraft precision approach trajectory to analyze the tightness of the proposed estimation error variance bound.

II. Overbounding Kalman Filter with Unknown Gauss-Markov Processes

Let $\hat{\mathbf{P}}$ be the Kalman filter (KF) estimate error covariance matrix and $\mathbf{P}$ be the true estimate error covariance matrix. The inequality $\hat{\mathbf{P}} \geq \mathbf{P}$ means that the predicted variance $\boldsymbol{\alpha}^T\hat{\mathbf{P}}\boldsymbol{\alpha}$ is greater than or equal to the true variance $\boldsymbol{\alpha}^T\mathbf{P}\boldsymbol{\alpha}$ for any real vector $\boldsymbol{\alpha}$.

Suppose that the measurement and process noise components are known to be first-order GMP. These processes are completely specified by a time constant τ, steady-state

978-1-7281-0244-3/20/$31.00 ©2020 IEEE

variance σ^2 and initial variance σ_0^2, and propagate according to the difference equation

$$a_{k+1} = e^{-\Delta t/\tau} a_k + \sqrt{\sigma^2 \left(1 - e^{-2\Delta t/\tau}\right)} w_k\,, \qquad w_k \sim \mathrm{WGN}\,(0,1) \;\text{ and }\; a_0 \sim N(0, \sigma_0^2) \tag{1}$$

where k is an arbitrary time index and $\Delta t = t_{k+1} - t_k$ is the discrete-time sampling interval. The notation $\mathrm{WGN}(0,1)$ indicates zero-mean white Gaussian noise with unit variance and $N(0, \sigma_0^2)$ denotes a zero-mean normal random variable with variance σ_0^2.

It was proved in [9] that when τ and σ^2 are only known to reside in the intervals $[\tau_{\min}, \tau_{\max}]$ and $[0, \sigma^2_{\max}]$, a state-augmented KF that models a_k with

$$\begin{aligned} \hat{\tau} &= \tau_{\max} \\ \hat{\sigma}^2 &= \sigma^2_{\max}(\tau_{\max}/\tau_{\min}) \\ \hat{\sigma}_0^2 &\geq \frac{2\sigma^2_{\max}}{1 + (\tau_{\min}/\tau_{\max})} \end{aligned} \tag{2}$$

is guaranteed to produce a covariance matrix $\hat{\mathbf{P}} \geq \mathbf{P}$.

A direct interpretation is that the design of the GMP that produces an overbounded covariance estimation must consider the maximum time constant from within the possible range and must inflate the steady-state maximum variance by a factor which is the ratio between the maximum and minimum time constant. Please note that when $\sigma_0^2 = \sigma^2_{\max}(\tau_{\max}/\tau_{\min})$, the overbounding augmented state error model is stationary. When using the lower bound for σ_0^2 in Equation (2), the GMP variance will have a transition phase until it converges to its steady state variance. Appendix A provides further insight about the nature of this bound with respect to the uncertain GMPs by representing it in different domains.

III. Error Model Implementation

In the following section, we describe the error models for the GNSS and IMU measurements. Particularly relevant for this paper is the consideration of uncertain time constants for the time correlated errors in GNSS, which we assume to reside within a known range of values.

A. GNSS

The linearized iono-free code and carrier measurement can be expressed as:

$$\rho_k^{i,j} - \tilde{\rho}_k^{i,j}(\mathbf{x}_{0,k}) = \mathbf{u}_k^{i,j^T} \Delta\mathbf{x}_k + b_k^j + \Delta S_k^{i,j} + T_k^{i,j} + mp_{\rho,k}^{i,j} + \epsilon_{\rho,k}^{i,j} \tag{3}$$

$$\phi_k^{i,j} - \tilde{\phi}_k^{i,j}(\mathbf{x}_{0,k}) = \mathbf{u}_k^{i,j^T} \Delta\mathbf{x}_k + b_k^j + \Delta S_k^{i,j} + T_k^{i,j} + N_\phi^{i,j} + mp_{\phi,k}^{i,j} + \epsilon_{\phi,k}^{i,j} \tag{4}$$

where $\rho_k^{i,j}$ is the code measurement of satellite i of constellation j at time epoch k. $\mathbf{u}_k^{i,j^T}$ is a unit line of sight vector user to satellite, $\Delta\mathbf{x}_k$ is the user position with respect to the linearization point. The receiver clock offset with respect to constellation j is b_k^j. $\Delta S_k^{i,j}$ is the residual satellite clock and ephemeris error after correction based on broadcast ephemeris, $T_k^{i,j}$ is the tropospheric error, $mp_{\rho,k}^{i,j}$ and $mp_{\phi,k}^{i,j}$ the multipath error in code and carrier respectively, $\epsilon_k^{i,j}$ the receiver noise and $N_\phi^{i,j}$ is the float iono-free integer ambiguity.

1) Satellite Clock and Orbit Errors: According to [11], we can model the residual satellite clock and ephemeris error for a satellite i as a Gauss-Markov process expressed as:

$$\Delta S^{i,GPS} \sim \mathcal{GM}(\sigma^2_{\mathrm{URA}}\ , \tau \in [4, 50] \text{ hours}), \tag{5}$$

$$\Delta S^{i,GAL} \sim \mathcal{GM}(\sigma^2_{\mathrm{URA}}\ , \tau \in [2, 38] \text{ hours}). \tag{6}$$

The user range accuracy (URA) is nominally chosen to be $\sigma_{\mathrm{URA}} = 1\mathrm{m}$ [12].

2) Tropospheric Errors: The largest part of the tropospheric error caused by the dry component can be removed by applying standard models [13]. The remaining wet component of the troposphere is more unpredictable and it is typically modeled as:

$$\Delta T_k^{i,j} = m_{\mathrm{tropo}}(\theta^{i,j}) \cdot \eta_{\mathrm{tropo},k}, \tag{7}$$

where $m(\theta^{i,j})$ is a mapping function that depends on the satellite elevation $\theta^{i,j}$ [13]:

$$m(\theta^{i,j}) = \frac{1.001}{\sqrt{0.002001 + \sin(\theta^{i,j})^2}}. \tag{8}$$

The uncertain component $\eta_{tropo,k}$ at the zenit is specified in [13] to be overbounded by a zero mean Gaussian distribution with variance $\sigma^2_{\mathrm{tropo}} = (0.12)^2\mathrm{m}^2$. In this work, we model the random component $\eta_{tropo,k}$ as a first-order Gauss-Markov process with the range of parameters specified in Table I.

3) Multipath and antenna group delay: For 100 seconds carrier-smoothed code, the following expression is given for the multipath error standard deviation [12]:

$$\sigma_{mp,\rho,\mathrm{sm}}^{i,j} = \sqrt{\frac{(f_{\mathrm{L1}}^2 - f_{\mathrm{L5}}^2)^2}{f_{\mathrm{L1}}^4 + f_{\mathrm{L5}}^4}} \left(0.13 + 0.53 e^{-\theta_{\mathrm{deg}}^{i,j}/10}\right), \tag{9}$$

where f_{L1} and f_{L5} are the GNSS carrier frequencies for L1 and L5 signals respectively.

We want to consider unsmoothed measurements in order to avoid the artificial correlation that the smoothing would cause between the measurements in the filter. It is found in [14, 15], that the unsmoothed code and carrier phase standard deviation due to multipath can be obtained with the following scaling of the smoothed ones:

$$\begin{aligned} \sigma_{mp,\rho} &= 1.5 \cdot \sigma_{mp,\rho,\mathrm{sm}}, \\ \sigma_{mp,\phi} &= 0.015 \cdot \sigma_{mp,\rho,\mathrm{sm}}. \end{aligned} \tag{10}$$

In this work, we model the total multipath for code and carrier as:

$$mp_{\rho,k}^{i,j} = \sigma_\rho(\theta_k^{i,j}) \cdot \eta_{mp_\rho,k}^{i,j}, \tag{11}$$

$$mp_{\phi,k}^{i,j} = \sigma_\phi(\theta_k^{i,j}) \cdot \eta_{mp_\phi,k}^{i,j}. \tag{12}$$

The first term will follow Equation (10) and it is used as a mapping or scaled parameter. The stochastic process $\eta^{i,j}_{mp_\rho,k}$ and $\eta^{i,j}_{mp_\phi,k}$ are modeled as first-order Gauss-Markov processes with unit variance and time-correlations in the ranges specified in Table I. Airborne multipath models for new signals and constellations are currently under development [16] and will be included in future publications.

4) Receiver Noise: The receiver noise component in the code and carrier measurement is modeled as a zero mean white Gaussian noise. Receiver code and carrier phase standard deviations can be expressed as [15]:

$$\begin{aligned}\sigma^{i,j}_{\epsilon_\rho} &= 19.6 \cdot \sigma^{i.j}_{\epsilon_\rho,\mathrm{sm}}, \\ \sigma^{i,j}_{\epsilon_\phi} &= 0.196 \cdot \sigma^{i.j}_{\epsilon_\rho,\mathrm{sm}},\end{aligned} \tag{13}$$

where $\sigma^{i.j}_{\epsilon_\rho,\mathrm{sm}}$ is the iono-free scaled carrier smoothed code noise standard deviation which is dependent on elevation [12]:

$$\sigma^{i.j}_{\epsilon_\rho,\mathrm{sm}} = \sqrt{\frac{(f^2_{\mathrm{L1}} - f^2_{\mathrm{L5}})^2}{f^4_{\mathrm{L1}} + f^4_{\mathrm{L5}}}} \left(0.15 + 0.43 e^{-\theta^{i,j}_{\mathrm{deg}}/6.9}\right). \tag{14}$$

5) Receiver Clock: GNSS receiver clocks are typically quartz oscillators; their offset with respect to GPS time is often treated as a parameter to be estimated. In this paper, we conservatively assume that at any particular time, we do not have any prior knowledge of the clock bias from previous time instants. This is modeled as an KF state parameter following a random walk with infinite (very high) variance.

TABLE I: GNSS Error Model Parameters.

		Error Model Parameters		
Error source	Mapping	Variance	τ_{min}	τ_{max}
Clock and Eph. (GPS)	-	$1\mathrm{m}^2$	4 h.	50 h.
Clock and Eph. (Gal)	-	$1\mathrm{m}^2$	2 h.	38 h.
Tropospheric	Eq.(8)	$(0.12\ \mathrm{m})^2$	900 s	2700 s
Raw Code Multipath	Eqs.(9,10)	$1\mathrm{m}^2$	10 s	900 s
Raw Carrier Multipath	Eqs.(9,10)	$1\mathrm{m}^2$	10 s	900 s
Receiver Code Noise	-	Eqs.(13,14)	-	-
Receiver Carrier Noise	-	Eqs.(13,14)	-	-

B. Inertial Measurement Unit (IMU)

The inertial measurements coming from gyroscopes and accelerometers are typically modeled as a combination of error sources and processes. First, we consider deterministic errors including misalignment of the sensor axis, scaling factors and constant biases. In this paper, we assume that these errors can be estimated and compensated for using an offline calibration procedure. Second, we consider stochastic errors that cannot be compensated for. A widely-used approach is to model stochastic errors of the IMU as the sum of a random constant turn-on bias, a time-correlated process and a white-Gaussian noise. We can therefore express the turn rate and specific force measurements as:

$$\tilde{\mathbf{w}}^b = \mathbf{w}^b + \mathbf{b}_{w,0} + \mathbf{b}_w + \boldsymbol{\eta}_w, \tag{15}$$

$$\tilde{\mathbf{f}}^b = \mathbf{f}^b + \mathbf{b}_{f,0} + \mathbf{b}_f + \boldsymbol{\eta}_f, \tag{16}$$

where $\tilde{\mathbf{w}}^b$ and $\tilde{\mathbf{f}}^b$ are the 3-axis measured turn rates and specific forces in a body frame b, respectively; similar, $\mathbf{w}^b$ and $\mathbf{f}^b$ are their true values, $\mathbf{b}_{\star,0}$ is the turn-on random constant bias with $\star$ referring either to the turn rates $\mathbf{w}$ or to the specific forces $\mathbf{f}$. Last, $\mathbf{b}_\star$ is the time-correlated bias and $\boldsymbol{\eta}_\star$ are the white Gaussian noise vectors of the associated measurements.

The turn-on biases can initially roughly be estimated by a coarse alignment process and further improved using a fine alignment process [17]. For low cost sensors in particular, final estimation of these random constant biases is often performed while in operation and thanks to the dynamics of the vehicle. In Section "Analysis of Overbounded GPS/INS", we will assume that some previous estimation process was available that provided initial values for these biases.

The most widely used model for the time-correlated bias of IMU measurements is based on a GM approximation, in part because it can easily by incorporated in a Kalman filter by state augmentation. This model is also adopted in this paper. Typical GM model parameter values for two sensor grades are listed in Table II and Table III for the GM bias over time (including a time constant and driving noise specifications) and for the measurement white noise.

TABLE II: IMU Accelerometer Error Parameters.

Grade	**Noise** $[\mu\mathrm{g}/\sqrt{\mathrm{Hz}}]$	**Bias Noise** [µg]	τ [s]
Navigation	15	20	3000
Tactical	50	160	3000

TABLE III: IMU Gyroscope Error Parameters.

Grade	**Noise** $[^\circ/\mathrm{h}/\sqrt{\mathrm{Hz}}]$	**Bias Noise** $[^\circ\,\mathrm{h}^{-1}]$	τ [s]
Navigation	0.01	0.005	12000
Tactical	2	0.5	10000

In this paper, we assume that the IMU error parameters are known. Future work will include the possibility to account for uncertainty in parameter values of the stochastic error models. This will capture the fact that error processes are not always repeatable, and that error behavior becomes unpredictable in the presence of variations in temperature and vibrations.

IV. GNSS/INS Kalman Filter Design

We consider a tightly coupled integration between GNSS and Inertial Navigation System (INS) where we use an error-state Kalman Filter. A general architecture of the system design is depicted in Figure 1. Note that the INS system is run outside the KF and it is *calibrated* with parameters estimated using the KF whenever an update step occurs.

A. State Selection

Kalman filter state parameters include position, velocity and attitude errors in a local navigation frame. In order to account for the time correlated errors present in IMU measurements we

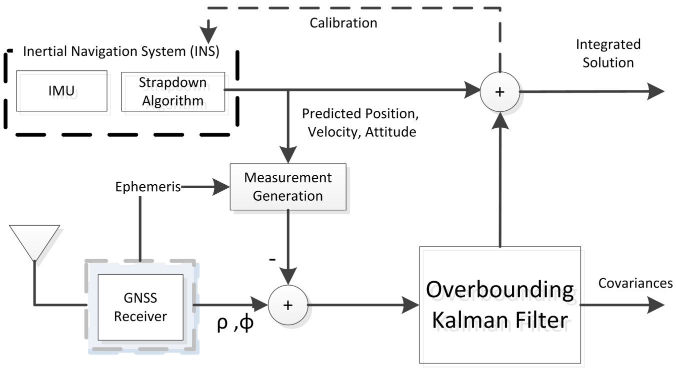

Fig. 1: GNSS/INS Kalman filter Architecture.

include the augmented states $\mathbf{b}_f$ and $\mathbf{b}_w$. The total number of error states related to the INS system are therefore $N_{\text{INS}} = 15$:

$$\mathbf{x}_{\text{INS}} = \begin{pmatrix} \delta\boldsymbol{\psi}^T & \delta\mathbf{v}^T & \delta\mathbf{p}^T & \mathbf{b}_f^T & \mathbf{b}_w^T \end{pmatrix}^T \tag{17}$$

where $\delta\boldsymbol{\psi}$, $\delta\mathbf{v}$ and $\delta\mathbf{p}$ are the 3D error in attitude, velocity and position of the INS system respectively. The filter states specific to GNSS first include the receiver clock biases with respect to each constellation in use. In order to account for the time correlated errors, additional augmented states are added to the state vector to capture the satellite clock and ephemeris, tropospheric and multipath error of each satellite. Finally, we add the integer ambiguities to each of the satellites in view. The GNSS-specific state vector component is therefore:

$$\mathbf{x}_{\text{GNSS}} = \begin{pmatrix} \mathbf{b}_{\text{clk}}{}^T & \boldsymbol{\Delta}\mathbf{S}^T & \mathbf{m}_{\text{tropo}}{}^T & \mathbf{mp}_\rho^T & \mathbf{mp}_\phi^T & \mathbf{N}_\phi{}^T \end{pmatrix}^T \tag{18}$$

where $\mathbf{b}_{\text{clk}}$ are the user clock biases for each GNSS constellation, $\boldsymbol{\Delta}\mathbf{S}$ the satellite ephemeris and clock error, $\mathbf{m}_{\text{tropo}}$ the tropospheric error at zenith, $\mathbf{mp}_\rho$ and $\mathbf{mp}_\phi$ the code and carrier multipath respectively and $\mathbf{N}_\phi$ the float iono-free integer ambiguities. The KF state vector therefore contains $N_{\text{KF}} = 15 + N_j + 5N_i$ parameters, where N_j is the number of constellations and N_i the number of satellites in view:

$$\mathbf{x}_{\text{KF}} = \begin{pmatrix} \mathbf{x}_{\text{INS}}^T & \mathbf{x}_{\text{GNSS}}^T \end{pmatrix}^T. \tag{19}$$

B. KF Prediction

The KF time-update or prediction step propagates the mean and covariance of the state estimates as follows:

$$\hat{\mathbf{x}}_{k|k-1} = \hat{\boldsymbol{\Phi}}_k \hat{\mathbf{x}}_{k-1|k-1}, \tag{20}$$

$$\hat{\mathbf{P}}_{k|k-1} = \hat{\boldsymbol{\Phi}}_k \hat{\mathbf{P}}_{k-1|k-1} \hat{\boldsymbol{\Phi}}_k^T + \mathbf{G}_k \hat{\mathbf{Q}}_k \mathbf{G}_k^T, \tag{21}$$

where $\hat{\mathbf{x}}_{k|k-1}$ and $\hat{\mathbf{P}}_{k|k-1}$ are the predicted states and covariance respectively, $\hat{\boldsymbol{\Phi}}_k$ is the time propagation matrix, $\hat{\mathbf{Q}}_k$ is the covariance of the process noise and $\mathbf{G}_k$ maps the process noise vector to the relevant states. The $(\hat{\ })$ notation on $\hat{\boldsymbol{\Phi}}_k$ and $\hat{\mathbf{Q}}_k$ indicates that a filter design choice is made: we want to set $\hat{\boldsymbol{\Phi}}_k$ and $\hat{\mathbf{Q}}_k$ guaranteeing that the computed estimate error covariance overbounds the actual estimation uncertainty. The discrete propagation matrix $\hat{\boldsymbol{\Phi}}_k$ for the GNSS/INS design can be expressed as:

$$\hat{\boldsymbol{\Phi}}_k = \begin{bmatrix} \boldsymbol{\Phi}_{k,\text{INS}} & \mathbf{0} \\ \mathbf{0} & \hat{\boldsymbol{\Phi}}_{k,\text{GNSS}} \end{bmatrix}, \tag{22}$$

where

$$\boldsymbol{\Phi}_{k,\text{INS}} = e^{\mathbf{F}_{k,\text{INS}}\Delta t} \approx \mathbf{I} + \mathbf{F}_{k,\text{INS}}\Delta t. \tag{23}$$

The Jacobian matrix $\mathbf{F}_{k,\text{INS}}$ can be obtained by differentiating the strapdown inertial differential equations at time k. This matrix is well known and can be found in textbooks on inertial integration (for instance, in [17]). It is worth noticing that $\boldsymbol{\Phi}_{\text{INS}}$ and $\mathbf{F}_{\text{INS}}$ do not have the $(\hat{\ })$ notation because, in this paper, the IMU error process parameters are assumed to be known. This assumption will be relaxed in future work.

The propagation design matrix $\hat{\boldsymbol{\Phi}}_{k,\text{GNSS}}$ is a diagonal matrix expressed as:

$$\hat{\boldsymbol{\Phi}}_{k,\text{GNSS}} = \begin{bmatrix} \mathbf{I}^{N_j\times N_j} & & & & & \\ & e^{-\Delta t/\hat{\tau}_{\Delta S}}\mathbf{I}^{N_i\times N_i} & & & & \\ & & e^{-\Delta t/\hat{\tau}_{\text{tropo}}}\mathbf{I}^{N_i\times N_i} & & & \\ & & & e^{-\Delta t/\hat{\tau}_{mp,\rho}}\mathbf{I}^{N_i\times N_i} & & \\ & & & & e^{-\Delta t/\hat{\tau}_{mp,\phi}}\mathbf{I}^{N_i\times N_i} & \\ & & & & & \mathbf{I}^{N_i\times N_i} \end{bmatrix}. \tag{24}$$

In Equation (21), the $\hat{\mathbf{Q}}_k$ matrix can also be split into contributions from the IMU and GNSS error processes using the following definitions:

$$\hat{\mathbf{Q}}_k = \begin{bmatrix} \mathbf{Q}_{\text{IMU}} & \mathbf{0} \\ \mathbf{0} & \hat{\mathbf{Q}}_{k,\text{GNSS}} \end{bmatrix}. \tag{25}$$

The covariance $\mathbf{Q}_{\text{IMU}}$ contains the IMU noise and GM variances which are not changing at different epochs.

The matrix $\hat{\mathbf{Q}}_{k,\text{GNSS}}$ is a diagonal matrix expressed as:

$$\hat{\mathbf{Q}}_{k,\text{GNSS}} = \text{diag}\left(\begin{bmatrix} \sigma_{\text{clk}}^2 \Delta t \mathbf{1}^{N_j\times 1} \\ \hat{\sigma}_{\Delta S}^2 \left(1 - e^{-\frac{2\Delta t}{\hat{\tau}_{\Delta S}}}\right) \mathbf{1}^{N_i\times 1} \\ \hat{\sigma}_{\text{tropo}}^2 \left(1 - e^{-\frac{2\Delta t}{\hat{\tau}_{\text{tropo}}}}\right) \mathbf{1}^{N_i\times 1} \\ \hat{\sigma}_{mp,\rho}^2 \left(1 - e^{-\frac{2\Delta t}{\hat{\tau}_{mp,\rho}}}\right) \mathbf{1}^{N_i\times 1} \\ \hat{\sigma}_{mp,\phi}^2 \left(1 - e^{-\frac{2\Delta t}{\hat{\tau}_{mp,\phi}}}\right) \mathbf{1}^{N_i\times 1} \\ \mathbf{0}^{N_i\times 1} \end{bmatrix}^T \right). \tag{26}$$

The notation $\mathbf{1}^{a\times b}$ and $\mathbf{0}^{a\times b}$ indicates a matrix (or vector) of size $a \times b$ filled with ones or zeros respectively. The values of the $\hat{\sigma}^2$ and $\hat{\tau}$ parameters are computed using Equation (2) and parameter range limits in Section III to ensure that the KF estimation is overbounded. Finally, matrix $\mathbf{G}_k$ can be written as:

$$\mathbf{G}_k = \begin{bmatrix} \mathbf{G}_{k,\text{IMU}} & \mathbf{0}^{N_{\text{INS}}\times N_{\text{GNSS}}} \\ \mathbf{0}^{N_{\text{GNSS}}\times N_{\text{INS}}} & \mathbf{I}^{N_{\text{GNSS}}\times N_{\text{GNSS}}} \end{bmatrix}, \tag{27}$$

where $N_{\text{INS}} = 15$ and $N_{\text{GNSS}} = N_j + 5N_i$. Matrix $\mathbf{G}_{k,\text{IMU}}$ is given in Appendix in [18].

C. KF Update

The Kalman filter measurement update is performed using the following equations:

$$\hat{\mathbf{x}}_{k|k} = \hat{\mathbf{x}}_{k|k-1} + \hat{\mathbf{K}}_k \left(\mathbf{z}_k - \mathbf{H}_k \hat{\mathbf{x}}_{k|k-1}\right), \tag{28}$$

$$\hat{\mathbf{P}}_{k|k} = \left(\mathbf{I} - \hat{\mathbf{K}}_k \mathbf{H}_k\right) \hat{\mathbf{P}}_{k|k-1}, \tag{29}$$

where $\hat{\mathbf{K}}$ is the Kalman filter gain obtained using:

$$\hat{\mathbf{K}}_k = \hat{\mathbf{P}}_{k|k-1} \mathbf{H}_k^T \left(\mathbf{H}_k \hat{\mathbf{P}}_{k|k-1} \mathbf{H}_k^T + \mathbf{R}_k\right)^{-1}. \tag{30}$$

The linearized KF measurement vector $\mathbf{z}$ is made of the differences between the iono-free code and carrier phase measurements and their predicted values computed using the INS current position:

$$\mathbf{z}_k = \begin{bmatrix} \rho_k^1 - \rho_{k,\text{INS}}^1 \\ \vdots \\ \rho_k^{N_i} - \rho_{k,\text{INS}}^{N_i} \\ \phi_k^1 - \phi_{k,\text{INS}}^1 \\ \vdots \\ \phi_k^{N_i} - \phi_{k,\text{INS}}^{N_i} \end{bmatrix}. \tag{31}$$

The measurement matrix $\mathbf{H}$ projects the states into measurement space and is expressed as:

$$\mathbf{H}_k = \begin{bmatrix} \mathbf{0}^{6\times N_i} & \mathbf{0}^{6\times N_i} \\ \mathbf{U}_k^T & \mathbf{U}_k^T \\ \mathbf{0}^{6\times N_i} & \mathbf{0}^{6\times N_i} \\ \mathbf{1}_{\{s^i\in c^j\}}^{N_j\times N_i} & \mathbf{1}_{\{s^i\in c^j\}}^{N_j\times N_i} \\ \mathbf{I}^{N_i\times N_i} & \mathbf{I}^{N_i\times N_i} \\ \mathbf{M}_{\text{tropo}} & \mathbf{M}_{\text{tropo}} \\ \mathbf{M}_{mp,\rho} & \mathbf{0}^{N_i\times N_i} \\ \mathbf{0}^{N_i\times N_i} & \mathbf{M}_{mp,\phi} \\ \mathbf{0}^{N_i\times N_i} & \mathbf{I}^{N_i\times N_i} \end{bmatrix}^T, \tag{32}$$

where $\mathbf{U}_k \in \mathcal{R}^{N_i\times 3}$ contains the line-of-sight vectors related to each of the satellites in view. The diagonal matrix $\mathbf{M}_{\text{tropo}} \in \mathcal{R}^{N_i\times N_i}$ contains the tropospheric mapping function for each of the satellites depending on their elevation as in Equation (8). And the diagonal matrix $\mathbf{M}_{mp,\rho}, \mathbf{M}_{mp,\phi} \in \mathcal{R}^{N_i\times N_i}$ contains the scaling of the multipath time-correlated errors according to their elevation as in Equation (10) for the code and carrier phase measurement respectively. Each element (j, i) of the matrix $\mathbf{1}_{\{s^i\in c^j\}}^{N_j\times N_i}$ is one if the satellite s^i belongs to constellation c_j and zero otherwise. Finally, $\mathbf{R}_k$ is a diagonal matrix containing the code and carrier receiver noise variances (Equation (13)):

$$\mathbf{R}_k = \begin{bmatrix} \sigma_{\epsilon_\rho}^2 \mathbf{I}^{N_i\times N_i} & \mathbf{0} \\ \mathbf{0} & \sigma_{\epsilon_\phi}^2 \mathbf{I}^{N_i\times N_i} \end{bmatrix}. \tag{33}$$

Note that in the case of loss of satellites in view, the size of state vector and covariance matrix must be reduced accordingly. Similarly, new states must be created and initialized if new satellites are available during the filter runtime. The change of satellites in view also affect the size of $\hat{\mathbf{\Phi}}_{k,\text{GNSS}}$, $\hat{\mathbf{Q}}_{k,\text{GNSS}}$, $\mathbf{G}_k$, $\mathbf{H}_k$ and $\mathbf{R}_k$.

V. Analysis of Overbounded GPS/INS

A. Precision Approach Simulation

In order to evaluate the behavior of a GPS/INS system in a realistic operational scenario, we consider the simulated precision approach procedure shown in Figure 2. We consider a half race-track procedure starting from a holding position at 7000ft with 200 knots speed. For the turn, the bank angle is at its maximum of 25 degrees as specified in [19], which is a worst case trajectory (i.e., high likelihood of losing visible low-elevation satellites due to banking). More realistic procedures could be defined based on true airspeed and tailwind, but these are beyond the scope of this work.

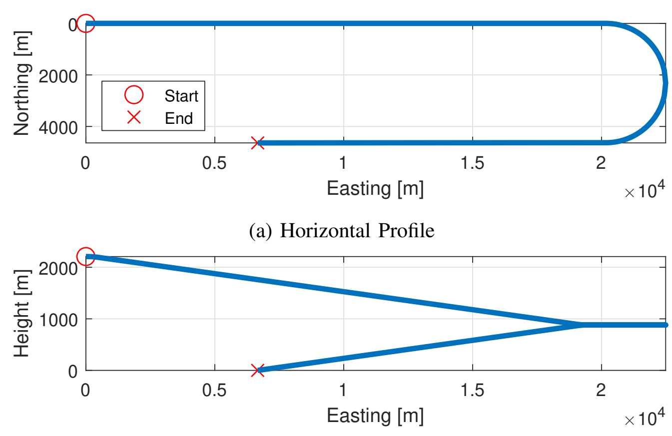

(a) Horizontal Profile

(b) Height profile

Fig. 2: Simulated Approach Trajectory.

We consider the integration of navigation grade IMU measurements at 100 Hz frequency with L1/L5 GPS code and carrier measurements at 1 Hz.

B. Linearized GPS/INS and KF Initialization

In order to evaluate the overbounding capability of the proposed solution, we implement a Linearized Kalman Filter (LKF) [17], linearized about the true trajectory. This helps isolate and properly evaluate the impact of the computed KF covariance as compared to the true covariance without including linearization errors of the Extended Kalman Filter (EKF). We can assume that when a simulated approach in Figure 2 is initiated, the navigation filter must have been running for a significant period of time. Finding realistic values for the initialized KF while limiting computation load is not trivial. We have selected the following values for the initial covariance matrix $\mathbf{P}_0$ related to the INS states:

$$\begin{aligned}
\mathbf{P}_{0,\delta\boldsymbol{\psi}} &= \text{diag}(0.01^2, 0.01^2, 0.03^2)\ \text{deg}^2,\\
\mathbf{P}_{0,\delta\mathbf{v}} &= \text{diag}(0.005^2, 0.005^2, 0.005^2)\ (\text{m/s})^2,\\
\mathbf{P}_{0,\delta\mathbf{p}} &= \text{diag}(1.2^2, 1.2^2, 1.2^2)\ \text{m}^2,\\
\mathbf{P}_{0,\delta\mathbf{b}_f} &= \text{diag}((10^{-3})^2, (10^{-3})^2, (10^{-4})^2)\ (\text{m/s/s})^2,\\
\mathbf{P}_{0,\delta\mathbf{b}_w} &= \text{diag}((10^{-5})^2, (10^{-5})^2, (10^{-4})^2)\ (\text{deg/s})^2
\end{aligned}$$

and for the GNSS states:

$$\begin{aligned}
\sigma^2_{0,\text{clk}} &= 1\ \text{m}^2,\\
\sigma^2_{0,\Delta S} &= 12.5\ \text{m}^2,\\
\sigma^2_{0,m_{\text{tropo}}} &= 0.0432\ \text{m}^2,\\
\sigma^2_{0,mp_\rho} &= 90\ \text{m}^2,\\
\sigma^2_{0,mp_\phi} &= 90\ \text{m}^2,\\
\sigma^2_{0,N_\phi} &= 0.6^2\text{m}^2.
\end{aligned}$$

The initial variance for the augmented states were selected according to the stationary bound variance from Equation (2). Notice that when we acquire new satellites during the simulation, we need to incorporate new augmented states for the correlated errors related to each satellites and the initialization is here performed with the non-stationary GM bound condition to minimize the uncertainty.

C. Covariance Analysis Results

The position covariance estimated using the proposed GPS/INS filter are depicted over time in Figure 3.

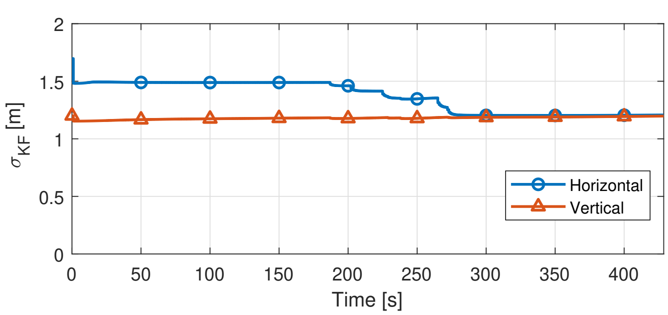

Fig. 3: Horizontal and vertical standard deviation estimated by the overbounding GPS/INS filter.

If the true time correlation of the GNSS errors is known, it is possible to compute the actual true KF estimation error covariance in addition to the computed covariance. Appendix B describes a method to derive the true error covariance for a generic discrete-time KF, which also applies to this aircraft navigation problem. In Figure 4, we compare the estimated positioning standard deviation with the true error standard deviation, assuming that the true values of the error correlation time constants are in the middle of the range of possible time constant values.

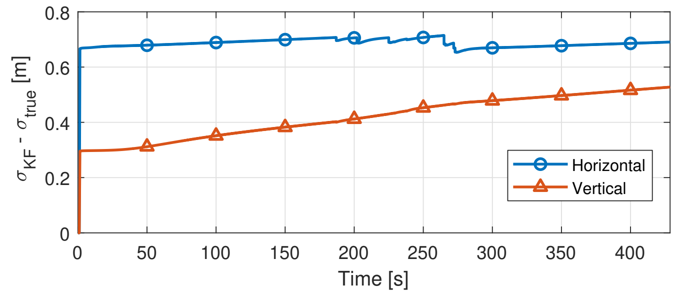

Fig. 4: Estimated KF standard deviation minus true error standard deviation. Here it is assumed that the true time correlations for each of the augmented states are in the middle of the range provided in Table I.

In Figure 4, the fact that the curves are positive for all simulated time epochs shows that the designed KF achieves bounding estimation covariance. The proof that this holds true for any values of the correlation time constants is provided in [9]. Figure 4 illustrates that this theoretical result holds true for practical GPS/INS integration applications. The results from Figure 3 and Figure 4 show that, in this example, the proposed filter produces estimated positioning standard deviations up to 70 cm larger than the true values in both horizontal and vertical directions. Although this value is a significant fraction of the actual true error standard deviation (also sub-meter level), the estimated total uncertainty is kept at the meter level. This has therefore the potential to support the computation of protection levels that satisfy stringent integrity and availability requirements for precision approach.

VI. Conclusions

The concept of overbounding has been developed and is in use in the context of civil aviation for snapshot estimators. The use of sequential estimators like the Kalman filter can potentially provide better performance in accuracy, continuity and availability than snapshot algorithms, especially when integrating information from multiple sensors. However, extending the concept of overbounding to GNSS/INS is challenging because time-correlated errors must be rigorously accounted for. In this paper, we provided a first solution to overbounding GNSS/INS estimation error variance in the presence of uncertain GNSS measurement errors behaving as Gauss-Markov processes (GMP). Our proposed integration scheme only causes minor changes in algorithms that already incorporated GMP error models but, in addition, produces guaranteed estimation error bounds which are essential for safety-critical applications.

Appendix A
Gauss-Markov Bound Interpretation

The methodology to bound the Kalman filter under uncertain GM errors consists on designing the augmented time correlated states with another GM process as specified in Equation (2).

There are different mathematical tools that are typically used to model the errors in sensor measurements. Depending on the type of sensor, the nature of the measurements and the specific parameters and time correlation that they have, one or another tool would be more suitable to perform the error modeling. In this appendix we include the representation of the proposed bound in [9] and Equation (2) in the following domains: Autocorrelation, Power Spectral Density (PSD) and Allan Variance.

A. Autocorrelation

The autocorrelation of a given stationary GM process with variance σ^2 and time correlation τ is expressed as:

$$R(\Delta t) = \sigma^2 e^{-\frac{|\Delta t|}{\tau}}, \tag{34}$$

where Δt is the sampling interval. In Figure 5, we can see some examples of different GM processes in the autocorrelation domain that have $\sigma^2 = 1$ and $\tau \in [1, 10]s$. In Figure 5, the

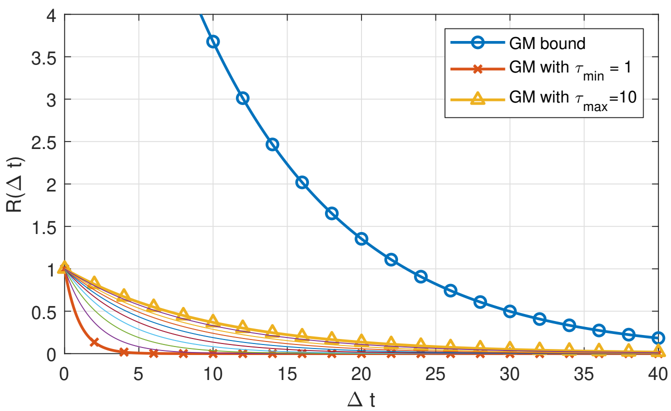

Fig. 5: Autocorrelation of GM processes with $\sigma^2 = 1$ and $\tau \in [1, 10]s$ and the GM process bound.

value of the autocorrelation of the bound at zero is expressed as $R(0) = \sigma^2 \frac{\tau_{\max}}{\tau_{\min}}$ and its value is therefore 10 for this example. Please note that the bound appears to be quite conservative for small sample intervals. This can be partially improved by using the non-stationary bound with a tighter initial variance as described in Section II.

B. Power Spectral Density (PSD)

The spectral density of a GM process for a given frequency f can be expressed as [20]:

$$S(f) = \frac{2\sigma^2/\tau}{(2\pi f)^2 + (1/\tau)^2}. \tag{35}$$

In Figure 6, the GMPs and the proposed bound are represented in the PSD domain. Please note that the GMPs with the uncertain time-correlation constant crosses at different frequencies, which supports the reason why choosing the GMPs with the highest time constant does not guaranteed an estimation bound. The PSD offers a powerful insight of the underlying error process in the frequency domain. In [21], the authors present a general overbounding methodology in the frequency domain

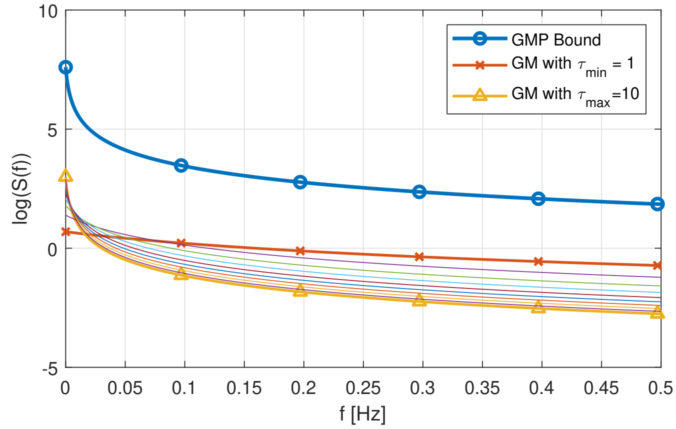

Fig. 6: Power Spectral Density (PSD) of GM processes with with $\sigma^2 = 1$ and $\tau \in [1, 10]s$ and the GM process bound.

for time-correlated error processes that goes beyond the Gauss-Markov error structure.

C. Allan Variance

The Allan variance (AV) is a statistical analysis tool to identify and characterize stochastic processes by observing their behaviour over different time periods [22]. The GMP in the AV domain has the following expression [22]:

$$\sigma^2_{\text{AV}}(\Delta t) = \frac{2\sigma^2\tau}{\Delta t}\left[1 - \frac{\tau}{2\Delta t}\left(3 - 4e^{\frac{-\Delta t}{\tau}} + e^{\frac{-2\Delta t}{\tau}}\right)\right] \tag{36}$$

where σ^2 is the GM steady state variance, τ is the time constant and Δt is the time interval under consideration.

Figure 7 represents the Allan deviation in log-log scale of GMPs with different time constants as well as the representation of the Equation (2) bound.

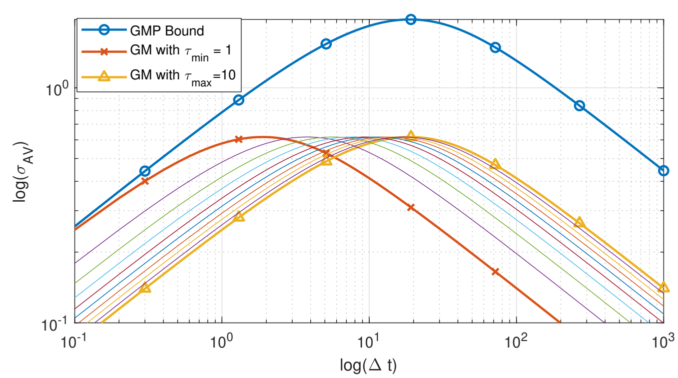

Fig. 7: Different Gauss-Markov Process with different time constant within $\tau \in [1, 10]$s in Allan Variance.

We can see that in fact the designed GMP is bounding the unknown process for any time interval for any possible time constant also in the AV domain. The maximum peak value of the bound is aligned with the one of the GMP with the maximum time constant, but its variance level is increased. This is consistent with the interpretation we did in Section II. This graphical representation also suggest that there is a tighter bound. Graphically this bound can be found by fitting a GMP that bounds in the AV domain both the *ascending slope* of the GMP with $\tau_{\min}$ and the *descending slope* of the GMP with $\tau_{\max}$. This new process is provided graphically in Figure 8.

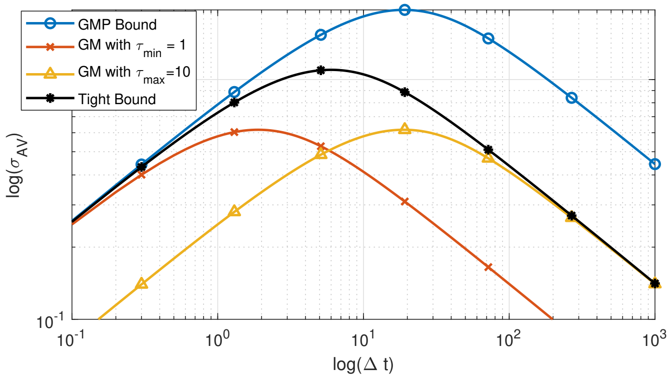

Fig. 8: New bound representation in Allan Variance Domain.

The new tighter bound can be found to have a time constant that is a mean value between the extremes of the range of possible time constants in the logarithmic scale:

$$\tau_b = 10^{\frac{log(\tau_{\min})+log(\tau_{\max})}{2}} = 10^{\frac{log(\tau_{\min}\tau_{\max})}{2}} \tag{37}$$

and the variance of the process must be inflated as:

$$\sigma_b^2 = \sigma_{\max}^2 \frac{\tau_b}{\tau_{\min}}. \tag{38}$$

This new bound is a candidate to provide a tighter bound over uncertain GMP and is first presented here only as a conjecture until the formal proof is published [23].

Appendix B
Discrete KF True error Covariance

The general discrete linear system we are working with can be described as follows:

$$\mathbf{x}_k = \mathbf{\Phi}\mathbf{x}_{k-1} + \mathbf{G}_k\mathbf{w}_k, \tag{39}$$
$$\mathbf{z}_k = \mathbf{H}_k\mathbf{x}_k + \boldsymbol{\nu}_k. \tag{40}$$

A Kalman filter estimator that designs *imperfectly* $\hat{\mathbf{\Phi}}$, and $\hat{\mathbf{Q}}$ with $E[\hat{\mathbf{w}}\hat{\mathbf{w}}^T] = \hat{\mathbf{Q}}$, can be written as:

$$\hat{\mathbf{x}}_{k|k-1} = \hat{\mathbf{\Phi}}\hat{\mathbf{x}}_{k-1|k-1}, \tag{41}$$
$$\hat{\mathbf{P}}_{k|k-1} = \hat{\mathbf{\Phi}}_k\hat{\mathbf{P}}_{k-1|k-1}\hat{\mathbf{\Phi}}_k^T + \mathbf{G}_k\hat{\mathbf{Q}}_k\mathbf{G}_k^T, \tag{42}$$
$$\hat{\mathbf{K}}_k = \hat{\mathbf{P}}_{k|k-1}\mathbf{H}_k^T\left(\mathbf{H}_k\hat{\mathbf{P}}_{k|k-1}\mathbf{H}_k^T + \mathbf{R}_k\right)^{-1}, \tag{43}$$
$$\hat{\mathbf{x}}_{k|k} = \hat{\mathbf{x}}_{k|k-1} + \hat{\mathbf{K}}_k\left(\mathbf{z}_k - \mathbf{H}_k\hat{\mathbf{x}}_{k|k-1}\right), \tag{44}$$
$$\hat{\mathbf{P}}_{k|k} = \left(\mathbf{I} - \hat{\mathbf{K}}_k\mathbf{H}_k\right)\hat{\mathbf{P}}_{k|k-1}. \tag{45}$$

Notice that because the filter is imperfectly designed, the covariance matrix $\hat{\mathbf{P}}_{k|k}$ is not guaranteed to bound the actual true error present in $\hat{\mathbf{x}}_{k|k}$. In [24] a methodology is proposed to study the sensitivity of the imperfect modeling for a continuous Kalman filter. In [10] similar expressions can be found for the hybrid Kalman filter. In here we follow the same approach to derive the true covariance error for the complete discrete Kalman filter.

Let's consider the error vector $\mathbf{e} \hat{=} \hat{\mathbf{x}} - \mathbf{x}$. Using it and Equation (39), for the prediction step we can write:

$$\begin{aligned}\mathbf{e}_{k|k-1} &= \hat{\mathbf{x}}_{k|k-1} - \mathbf{x}_k \\ &= \hat{\mathbf{\Phi}}\hat{\mathbf{x}}_{k-1|k-1} - \mathbf{\Phi}\mathbf{x}_{k-1} - \mathbf{G}_k\mathbf{w}_k.\end{aligned} \tag{46}$$

Defining $\Delta\mathbf{\Phi} \hat{=} \hat{\mathbf{\Phi}} - \mathbf{\Phi}$, Equation (46) can be written as:

$$\mathbf{e}_{k|k-1} = \hat{\mathbf{\Phi}}\mathbf{e}_{k-1|k-1} + \Delta\mathbf{\Phi}\mathbf{x}_{k-1} - \mathbf{G}\mathbf{w}_k. \tag{47}$$

In order to propagate this error over time, we can consider the time propagation of the extended vector $\mathbf{x}^{\mathrm{e}} = \begin{bmatrix} \mathbf{e} & \mathbf{x} \end{bmatrix}^T$ as:

$$\begin{bmatrix} \mathbf{e}_{k|k-1} \\ \mathbf{x}_k \end{bmatrix} = \begin{bmatrix} \hat{\mathbf{\Phi}} & \Delta\mathbf{\Phi} \\ \mathbf{0} & \mathbf{\Phi} \end{bmatrix} \begin{bmatrix} \mathbf{e}_{k-1|k-1} \\ \mathbf{x}_{k-1} \end{bmatrix} + \begin{bmatrix} -\mathbf{G}_k\mathbf{w}_k \\ \mathbf{G}_k\mathbf{w}_k \end{bmatrix}, \tag{48}$$

whose associated covariance is:

$$\begin{aligned}\mathbf{P}^{\mathrm{e}}_{k|k-1} = &\begin{bmatrix} \hat{\mathbf{\Phi}} & \Delta\mathbf{\Phi} \\ \mathbf{0} & \mathbf{\Phi} \end{bmatrix} \mathbf{P}^{\mathrm{e}}_{k-1|k-1} \begin{bmatrix} \hat{\mathbf{\Phi}} & \Delta\mathbf{\Phi} \\ \mathbf{0} & \mathbf{\Phi} \end{bmatrix}^T \\ &+ \begin{bmatrix} \mathbf{G}_k\mathbf{Q}_k\mathbf{G}_k^T & -\mathbf{G}_k\mathbf{Q}_k\mathbf{G}_k^T \\ -\mathbf{G}_k\mathbf{Q}_k\mathbf{G}_k^T & \mathbf{G}_k\mathbf{Q}_k\mathbf{G}_k^T \end{bmatrix}.\end{aligned} \tag{49}$$

For the update step we proceed in a similar way:

$$\begin{aligned}\mathbf{e}_{k|k} = \hat{\mathbf{x}}_{k|k} - \mathbf{x}_k &= \left(\mathbf{I} - \hat{\mathbf{K}}_k\mathbf{H}_k\right)\hat{\mathbf{x}}_{k|k-1} + \hat{\mathbf{K}}_k\mathbf{z}_k - \mathbf{x}_k \\ &= \left(\mathbf{I} - \hat{\mathbf{K}}_k\mathbf{H}_k\right)\mathbf{e}_{k|k-1} - \hat{\mathbf{K}}_k\boldsymbol{\nu}_k,\end{aligned} \tag{50}$$

which leads to the extended update expression:

$$\begin{bmatrix} \mathbf{e}_{k|k} \\ \mathbf{x}_k \end{bmatrix} = \begin{bmatrix} \left(\mathbf{I} - \hat{\mathbf{K}}_k\mathbf{H}_k\right) & \mathbf{0} \\ \mathbf{0} & \mathbf{I} \end{bmatrix} \begin{bmatrix} \mathbf{e}_{k|k-1} \\ \mathbf{x}_k \end{bmatrix} + \begin{bmatrix} -\hat{\mathbf{K}}_k\boldsymbol{\nu}_k \\ \mathbf{0} \end{bmatrix} \tag{51}$$

and whose associated covariance is now:

$$\begin{aligned}\mathbf{P}^{\mathrm{e}}_{k|k} = &\begin{bmatrix} \left(\mathbf{I} - \hat{\mathbf{K}}_k\mathbf{H}_k\right) & \mathbf{0} \\ \mathbf{0} & \mathbf{I} \end{bmatrix} \mathbf{P}^{\mathrm{e}}_{k|k-1} \begin{bmatrix} \left(\mathbf{I} - \hat{\mathbf{K}}_k\mathbf{H}_k\right) & \mathbf{0} \\ \mathbf{0} & \mathbf{I} \end{bmatrix}^T \\ &+ \begin{bmatrix} \hat{\mathbf{K}}_k\mathbf{R}_k\hat{\mathbf{K}}_k^T & \mathbf{0} \\ \mathbf{0} & \mathbf{0} \end{bmatrix}.\end{aligned} \tag{52}$$

The true error covariance of the states of interest, i.e., $\mathbf{P} = E[\mathbf{e}\mathbf{e}^T]$ can be extracted from the upper block of the covariance matrix $\mathbf{P}^{\mathrm{e}}$.

Notice also that Equation (52) cannot be written in a simplified fashion as in Equation (45) because the covariance of the prediction of $\mathbf{e}_{k|k-1}$ is different from the one that is used to compute the Kalman gain, which is based on the *imperfectly* designed Kalman filter estimator.

Finally, the initial state covariance $\hat{\mathbf{P}}_0$ must be also set according to our design. Assuming an error state implementation of the filter where $E[\mathbf{x}_0] = 0$, the initialization of the extended matrix we used for the sensitivity analysis is described as:

$$\mathbf{P}_0^e = \begin{bmatrix} \mathbf{P}_0 & -\mathbf{P}_0 \\ -\mathbf{P}_0 & \mathbf{P} \end{bmatrix}. \tag{53}$$

Using Equation (53), Equation (49) and Equation (52) it is possible to obtain recursively the true error KF covariance matrix over time.

References

[1] M. Brenner, "Integrated GPS/Inertial Fault Detection Availability," *NAVIGATION*, vol. 43, no. 2, pp. 111–130, 1996.

[2] Çağatay Tanıl, S. Khanafseh, M. Joerger, and B. Pervan, "Sequential Integrity Monitoring for Kalman Filter Innovations-based Detectors," in *Proceedings of the 31st International Technical Meeting of the Satellite Division of The Institute of Navigation (ION GNSS+ 2018)*, Sep. 2018.

[3] O. García Crespillo, A. Grosch, J. Skaloud, and M. Meurer, "Innovation vs Residual KF Based GNSS/INS Autonomous Integrity Monitoring in Single Fault Scenario," in *ION GNSS+ 2017*, Portland, OR, USA, Sep. 2017.

[4] U. Bhatti and W. Ochieng, "Detecting Multiple Failures in GPS/INS Integrated System: A Novel Architecture for Integrity Monitoring," *Journal of Global Positioning Systems*, vol. 8, pp. 26–42, 06 2009.

[5] O. García Crespillo, A. Andreetti, and A. Grosch, "Design and Evaluation of Robust M-Estimators for GNSS Positioning in Urban Environments," in *2020 International Technical Meeting of The Institute of Navigation*, 2 2020.

[6] O. García Crespillo, D. Medina, J. Skaloud, and M. Meurer, "Tightly coupled GNSS/INS Integration based on Robust M-estimators," in *2018 IEEE/ION Position, Location and Navigation Symposium (PLANS)*. Monterey, CA: IEEE, Apr. 2018, pp. 1554–1561.

[7] D. A. Medina, M. Romanovas, I. Herrera-Pinzón, and R. Ziebold, "Robust Position and Velocity Estimation Methods in Integrated Navigation Systems for Inland Water Applications," in *2016 IEEE/ION Position, Location and Navigation Symposium (PLANS)*, 2016, pp. 491–501.

[8] J. Rife and B. Pervan, "Overbounding Revisited: Discrete Error-Distribution Modeling for Safety-Critical GPS Navigation," *IEEE Transactions on Aerospace and Electronic Systems*, vol. 48, no. 2, pp. 1537–1551, 2012.

[9] S. Langel, O. García Crespillo, and M. Joerger, "Bounding Sequential Estimation Errors due to Gauss-Markov Noise with Uncertain Parameters," in *Proceedings of the 32nd International Technical Meeting of the Satellite Division of The Institute of Navigation (ION GNSS+ 2019)*, September 2019.

[10] S. Langel, O. García Crespillo, and M. Joerger, "Overbounding the Effect of Uncertain Gauss-Markov Noise in Kalman Filtering," *unpublished*, 2020.

[12] Working Group C - ARAIM Subgroup , "Milestone 3 Report," EU/US Cooperation on Satellite Navigation, Tech. Rep., 2016.

[11] E. Gallon, M. Joerger, S. Perea, and B. Pervan, "Error Model Development for ARAIM Exploiting Satellite Motion," in *Proceedings of the 32nd International Technical Meeting of the Satellite Division of The Institute of Navigation (ION GNSS+ 2019)*, September 2019.

[13] RTCA/SC-159, "RTCA/DO-229C: Minimum Operational Performance Standards for Global Positioning System/Wide Area Augmenation System Airborne Equipment," RTCA, Tech. Rep., 2001.

[14] M. Joerger and B. Pervan, "Exploiting Satellite Motion in ARAIM: Measurement Error Model Refinement using Experimental Data," in *Proceedings of the 29th International Technical Meeting of The Satellite Division of the Institute of Navigation (ION GNSS+ 2016)*, September 2016.

[15] ——, "Multi-constellation ARAIM Exploiting Satellite Motion," *Navigation, Journal of the Institute of Navigation*, Jan. 2020.

[16] M.-S. Circiu, M. Felux, S. Caizzone, C. Enneking, F. Fohlmeister, M. Rippl, I. Gulie, D. R uegg, J. Griggs, R. Lazzerini, F. Hagemann, F. Tranchet, P. Bouniol, and M. Sgammini, "Airborne multipath models for dual-constellation dual-frequency aviation applications," in *ION ITM 2020*, Januar 2020.

[17] P. D. Groves, *Principles of GNSS, Inertial, and Multisensor Integrated Navigation Systems*, 2nd ed. Artech House, 2013.

[18] O. García Crespillo, A. Grosch, and M. Meurer, "Detection of DME Ranging Faults with INS Coupling," in *2017 Integrated Communication, Navigation and Surveillance Conference (ICNS)*, 2017.

[19] I. C. A. O. (ICAO), "DOC 8168: Procedures for Air Navigation Services - Aircraft Operations (PANS-OPS)," ICAO, Tech. Rep., 2006.

[20] R. G. Brown and P. Y. Hwang, *Introduction to random signals and applied Kalman filtering, 4th ed.* Wiley New York, 2012, vol. 3.

[21] S. Langel, O. García Crespillo, and M. Joerger, "A New Approach for Modeling Correlated Gaussian Errors using Frequency Domain Overbounding," in *Position, Navigation and Timing Symposium (PLANS)*, 5 2020.

[22] "IEEE Standard Specification Format Guide and Test Procedure for Single-Axis Interferometric Fiber Optic Gyros," *IEEE Std 952-1997*, pp. 1–84, Feb 1998.

[23] O. García Crespillo, M. Joerger, and S. Langel, "A tight bound for uncertain time-correlated errors with Gauss-Markov structure," *unpublished*, 2020.

[24] A. Gelb and T. A. S. Corporation, *Applied Optimal Estimation*. The MIT Press, 1974.